Marine and Petroleum Geology 72 (2016) 45–61

Contents lists available at ScienceDirect

Marine and Petroleum Geology

journal homepage: www.elsevier.com/locate/marpetgeo

Research paper

Diagenesis of the palaeo-oil-water transition zone in a Lower Pennsylvanian carbonate reservoir: Constraints from cathodoluminescence microscopy, microthermometry, and isotope geochemistry

A.N. Kolchugin [a], A. Immenhauser [b, *], B.F. Walter [c], V.P. Morozov [a]

[a] Kazan Federal University, Institute of Geology and Petroleum Technologies, Russia
[b] Ruhr-University Bochum, Faculty for Geosciences, Institute of Geology, Mineralogy and Geophysics, Germany
[c] Eberhard Karls University Tübingen, Department of Geoscience, Germany

ARTICLE INFO

Article history:
Received 20 July 2015
Received in revised form
11 January 2016
Accepted 13 January 2016
Available online 14 January 2016

Keywords:
Carbonate reservoirs
Diagenesis
Geochemistry
Hydrocarbons

ABSTRACT

Oil-water transition zones in carbonate reservoirs represent important but rarely studied diagenetic environments that are now increasingly re-evaluated because of their potentially large effects on reservoir economics. Here, data from cathodoluminescence and fluorescence microscopy, isotope geochemistry, microthermometry, and X-ray tomography are combined to decipher the diagenetic history of a 5-m-long core interval comprising the oil-water transition zone in a Lower Pennsylvanian carbonate reservoir. The aim is to document the cementation dynamics prior, during, and after oil emplacement in its context of changing fluid parameters. Intergrain porosity mean values of 7% are present in the upper two sub-zones of the oil-water transitions zone but values sharply increase to a mean of 14% in the lower sub-zone grading into the water-saturated portions of the reservoir and a very similar pattern is observed for permeability values. In the top of the water-filled zone, cavernous porosity with mean values of about 24% is found. Carbonate cements formed from the earliest marine to the late burial stage. Five calcite (Ca-1 through 5) and one dolomite (Dol) phase are recognized with phase Ca-4b recording the onset of hydrocarbon migration. Carbon and oxygen cross-plots clearly delineate different paragenetic phases with Ca-4 representing the most depleted $\delta^{13}C$ ratios with mean values of about −21‰. During the main phase of oil emplacement, arguably triggered by far-field Alpine tectonics, carbonate cementation was slowed down and eventually ceased in the presence of hydrocarbons and corrosive fluids with temperatures of 110–140 °C and a micro-hiatal surface formed in the paragenetic sequence. These observations support the "oil-inhibits-diagenesis" model. The presence an earlier corrosion surface between phase Ca-3 and 4 is best assigned to initial pulses of ascending corrosive fluids in advance of hydrocarbons. The short-lived nature of the oil migration event found here is rather uncommon when compared to other carbonate reservoirs. The study is relevant as it clearly documents the strengths of a combined petrographic and geochemical study in order to document the timing of oil migration in carbonate reservoirs and its related cementation dynamics.

1. Introduction

Reservoir oil-water transition zones (Christiansen et al., 2000; Heasley et al., 2000; Byrnes and Bhattacharya, 2006; Carnegie, 2006) are generally described as the intervals from which both oil and water are produced. Following the definition of Fanchi et al. (2002), the top of this interval is the elevation at which water-free oil is produced. The lower limit, although often gradual, is the shallowest depth at which oil-free water is present. In some reservoirs, the entire column is in a transition zone. In the past, oil-water transition zones, ranging in thickness from less than 1 to several 100 m, were considered non-economic and often not cored (Christiansen et al., 2000). More recently, however, oil-water transition zones in reservoir rocks worldwide have been

* Corresponding author.
E-mail address: adrian.immenhauser@rub.de (A. Immenhauser).

http://dx.doi.org/10.1016/j.marpetgeo.2016.01.014
0264-8172/

increasingly re-evaluated and are now considered significant because of their potentially large effects (>30% of the estimated original oil in place) on reservoir economics (Fanchi et al., 2002).

Burial diagenetic processes and products within the interstices of reservoir rocks (shelf carbonates, chalk, clastics etc.) are clearly non-trivial with regard to the processes involved as these take place in the presence of two immiscible fluids, here oil and water (Worden et al., 1998, 1999; Jesenius and Burruss, 1990; Helgeson et al., 1993; Heggheim et al., 2005; Risnes et al., 2003, 2005; Sathar et al., 2012). This holds particularly true in the case of often mixed-wet carbonate reservoirs. This is because hydrocarbons contain abundant polar organic compounds that interact with the carbonate minerals (Ingalls et al., 2004; Hao et al., 2015). As a consequence, work dealing with experimental approaches, field studies and modeling with focus on the relationship between water-saturation, pH, wettability and relative permeability abounds (Christiansen et al., 2000; Morrow and Mason, 2001; Zhang et al., 2007; Sathar et al., 2012; Al-Dhahli et al., 2014).

Considering the potential significance of the oil-water transition zone, however, the number of published case studies dealing specifically with the carbonate diagenetic pathways of rocks in this crucial interval is still remarkably limited (Sellwood et al., 1993; Neilson et al., 1998; Heasley et al., 2000). The comparable scarcity of detailed studies represents an important information gap given the fact that the in-depth analysis of the paragenetic succession at water-oil contacts allows for the assessment of the timing of petroleum migration relative to diagenetic and tectonic events both for carbonate and clastic reservoirs (Burruss et al., 1983; Sellwood et al., 1993; Helgeson et al., 1993; Worden et al., 1998; Cox et al., 2010). Moreover, the comprehensive study of Worden et al. (1998) discusses, albeit from the perspective of clastic reservoirs, two conflicting schools of mind one termed as “oil-inhibits-diagenesis-model”, the other as “oil-does-not-inhibits-diagenesis-model”. The “oil-inhibits-diagenesis” model predicts that early emplacement of oil will inhibit (quartz, clay mineral, or carbonate) cementation and related pressure solution and consequently, reservoir quality is preserved. Conversely, the “oil-does-not-inhibits-diagenesis” model suggests that oil migration and emplacement is no major control of diagenetic pathways and attributes excess porosity to other factors.

This study provides a detailed description and interpretation of carbonate paragenetic phases from core material of a selected Bashkirian (Lower Pennsylvanian, *ca* 323–315 Ma) limestone reservoir in the Volga-Ural region of Russia. The focus is on a 5-m-long core interval representing the palaeo-oil-water transition zone. Paragenetic phases are brought into a temporal, burial, and mechanistic context. Making use of the detailed cement stratigraphy across the oil-water-transition zone documented here, we address the following four main questions:

1. What is the relation between carbonate diagenesis and oil migration? Specifically, does oil emplacement inhibits carbonate cementation or not?
2. Is oil migration assigned to a single paragenetic phase or expanded over a significant portion of the diagenetic pathway of the reservoir rock studied?
3. Are diagenetic fluids during oil emplacement discernible – in terms of their temperature and chemistry – from ambient pore fluids prior to and after oil migration?

The data shown here are significant for the wider understanding of palaeo-oil-water transition zones in carbonate reservoirs in general and highlight the potential of petrographic, microthermometric, and geochemical tools applied studied to these critical reservoir intervals.

2. Geological setting and economic significance

The focus of this study is on Lower Bashkirian limestones from an oil field of the Nurlatsky district in the Republic of Tatarstan (Russian Federation; Fig. 1). The units cored are situated in the Melekesskaya depression located in the south-central part of the vast Precambrian Russian craton (Fig. 1; Hachatryan, 1979). Devonian, Carboniferous, and Lower Permian clastic and shallow water carbonate units, overlaying a weathered Proterozoic basement surface, form the predominant sedimentary succession (Fig. 1; Alekseev et al., 1996; Buggisch et al., 2011). The thickness of the Paleozoic cover reaches about 1900 m. Exposures in this region are only present along major river valleys and are restricted to Neogene and Quaternary rocks.

In terms of its geological setting, the core interval studied is from an oil field located in the eastern part of the East-European carbonate platform, forming portions of the Volga-Ural anticline (Fig. 2; Hachatryan, 1979; Voytovich and Gatiyatullin, 2003). Following Permian sedimentation, the Volga-Ural region experienced a phase of tectonically stability with only minor vertical tectonic movements and very limited sedimentation. From the Neogene onwards, a steady tectonic uplift lead to erosion and the formation of major alluvial depositional systems (thickness up 100–150 m). The main structures of the Volga-Ural anticline were formed as a result of this vertical basement uplift (Hachatryan, 1979; Mkrtchyan, 1980).

Economically significant carbonates reservoir units are concentrated in the Lower Mississippian and the Lower Pennsylvanian, with the Bashkirian units being one of the main carbonate target intervals in the Volga-Ural region (Fig. 3). From a production point of view, significant portions of the Devonian clastic reservoirs rocks are in a late production stage and consequently, the main focus of oil exploration in this region is now on the Carboniferous reservoir rocks. The source rocks of the oil fields in Volga-Ural region (Gordadze and Tikhomirov, 2005; Galimov and Kamaleeva, 2015) are Upper Devonian (Frasnian–Famennian) black shales (Aizenshtat et al., 1998). These units comprise thinly bedded calcareous-siliceous successions with abundant organic matter (Yudina et al., 2002; Gordadze and Tikhomirov, 2005).

3. Depositional environment, stratigraphy, and sedimentology

Accessible data in the international literature with focus on the Carboniferous of the Russian platform are scarce to absent. Here, we provide a brief overview of the facies types found and place our findings in the ramp model of Proust et al. (1998). During the Pennsylvanian and Early Permian, the Russian Platform was characterized in its eastern domains by a large, wave-dominated carbonate ramp and the subsiding foredeep of the Ural Mountains (Proust et al., 1998, Fig. 2). Within this ramp setting, the carbonates studied here were deposited. Based on palaeomagnetic and palaeoenvironmental data, the climate zone assigned to the Melekesskaya depression during Pennsylvanian times was semi-arid and (sub-)tropical (Proust et al., 1998). As recognized in Lower Pennsylvanian sections worldwide (Heckel, 1986; Soreghan and Giles, 1999), the relative sea level fluctuated repeatedly forming hiatal and karstified units on a regional scale. In the short core interval studied here, however, evidence for significant subaerial diagenesis is lacking.

With reference to the middle Carboniferous ramp of the Russian platform, Proust et al. (1998) subdivide inner, mid- and outer ramp facies. The definition used is such that the inner ramp environment is placed permanently above the effective fair-weather wave base, the middle ramp environment is situated between the effective

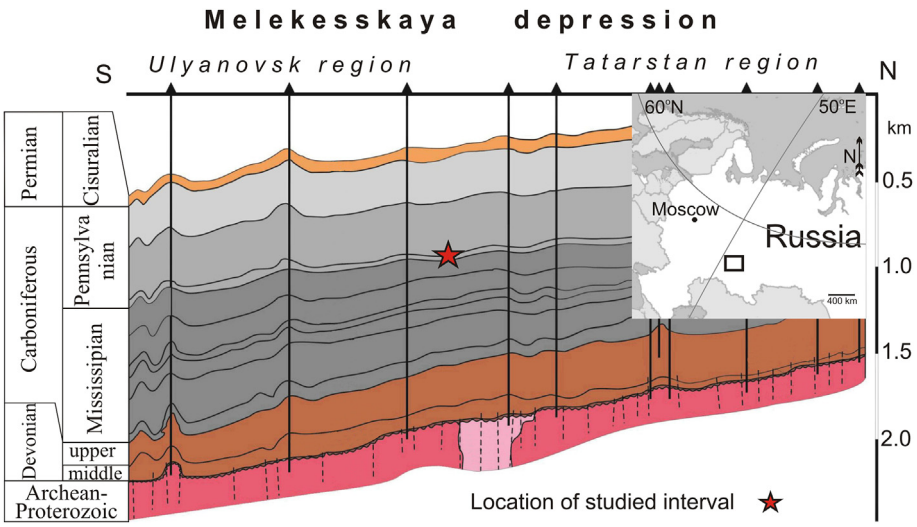

Fig. 1. Transect (south-north) across Melekesskaya depression with indication of main stratigraphic units and approximate indication of study window (modified after Gorunova, 2009). Small inset to upper right indicates position of study area.

storm and fair-weather wave base and the outer ramp is below situated near-permanently below the effective storm wave base with exceptional storm events resulting in wave base orbitals affecting fine-grained seafloor sediments (Immenhauser, 2009). The Bashkirian core portion (Fig. 3) studied in the context of this paper is best assigned a subtidal inner to middle ramp (Halymbadzha, 1962), characterized by normal marine seawater and small coral biostromes affected by occasional storm events. The presence of grainy facies, and specifically superficial ooids facies at some intervals (Fig. 4), points to frequent but not permanent (muddy facies) fair-weather or swell-wave base activity leading to entrainment and winnowing of fine-grained sediment. Evidence for an overall shallow, normal marine depositional setting comes from the overall subtidal mid-ramp biota including brachiopods, benthic foraminifera, crinoids or corals (Fig. 4; Bachtel and Dorobek, 1998; Burchette and Wright, 1992). In terms of the facies associations in the core studied here, these are best assigned to the "subtidal patch-reef and mud-flat lithofacies" of Proust et al. (1998, p. 1178). Small volumes of clastic detrital material are present in core material and include kaolinite in the clay insoluble material suggesting runoff (and/or aeolian transport) from emerged land in the regional vicinity (Kolchugin et al., 2013).

The main facies types found in the only 5-m-long section of Bashkirian core material across the oil-water transition zone studied here are bioclastic grainstones with coated grains and locally oncoidal-ooidal facies, bioclastic algal-foraminiferal packestones and less common, mud- and wackestones with abundant small and unspecified shell debris. In core samples, intact bivalve shells are locally found. At some intervals, coral framestone facies has been cored (Fig. 4E). Stratigraphically, the lower two section meters are characterized by an alternation of pack-to grainstones with two coral framestone intervals. Further upcore, poorly washed grainstones dominate the facies whilst the uppermost section meter is typified by wackestones.

3.1. Oil-water transition zone

Judging from a compilation of available well data, the oil-water transition zones in the stratigraphic interval studied range regionally in thickness from between 2 and 10 m. The present understanding is that the thickness of the transition zone depends on a series of factors that are interrelated in a non-trivial manner: (i) the position of the cored interval on the dome structure in the oil field. The thickness of the transition zone increases towards the dome center and decreases towards the flank of the dome; (ii) the productivity of the reservoir, specifically the thickness of the oil-saturated zone and spatial differences in oil saturation; (iii) the lateral and stratigraphic facies distribution across the oil field, with thicker oil-water transition zones (up to 10 m) in pack-to grainstone facies and stratigraphically thinner transition intervals (2 m and less) in wacke-to mudstone facies.

4. Methods

The core interval studied was drilled in June of 2013 but data sets on density, sonic, wettability, or geochemical data on gas phase CO_2 – now regularly compiled for more recently drilled wells – were either not compiled or are not available due to confidentiality reasons. Consequently, methods applied here focus on cathodoluminescence microscopy, micro-thermometry, and geochemical data complementing data on porosity, permeability, resistivity, and gamma ray (Ali, 1995; Kaufman et al., 1988; Bruckschen et al., 1992; Zeeh et al., 1995; Burley et al., 1989; Ehrenberg et al., 2002; Granier and Staffelbach, 2009; Carpentier et al., 2014). Below methods applied in this study are detailed. Data on resistivity and gamma ray are from the following sources (Gorbachev, 1990; Doveton, 1999; Khalil et al., 2015).

4.1. Isotope geochemistry

Matrix micrite and cement sub-samples were collected from core slabs, using a hand held drill with 1 mm diameter drill bits. The focus was on phase-specific cement data, hence only fabrics that were volumetrically significant enough to mechanically extract enough sample powder were selected. This refers mainly to late diagenetic fabrics. Cement data were complemented by a stratigraphic transect of bulk micrites sampled across the 5-m thick oil-water transition zone. A total of 25 carbon and oxygen isotope analyses were performed at the Ruhr University Bochum, Germany. For the analysis of C and O isotope ratios, between 0.27 and 0.33 mg of sample powder was dried in an oven at 105 °C for 48 h. Phosphoric acid (104%) was added to the sample, in a gasbench and then analyzed with a Finnigan MAT 253. Four repeat samples were analyzed for every sample batch of 48 samples. Adding the

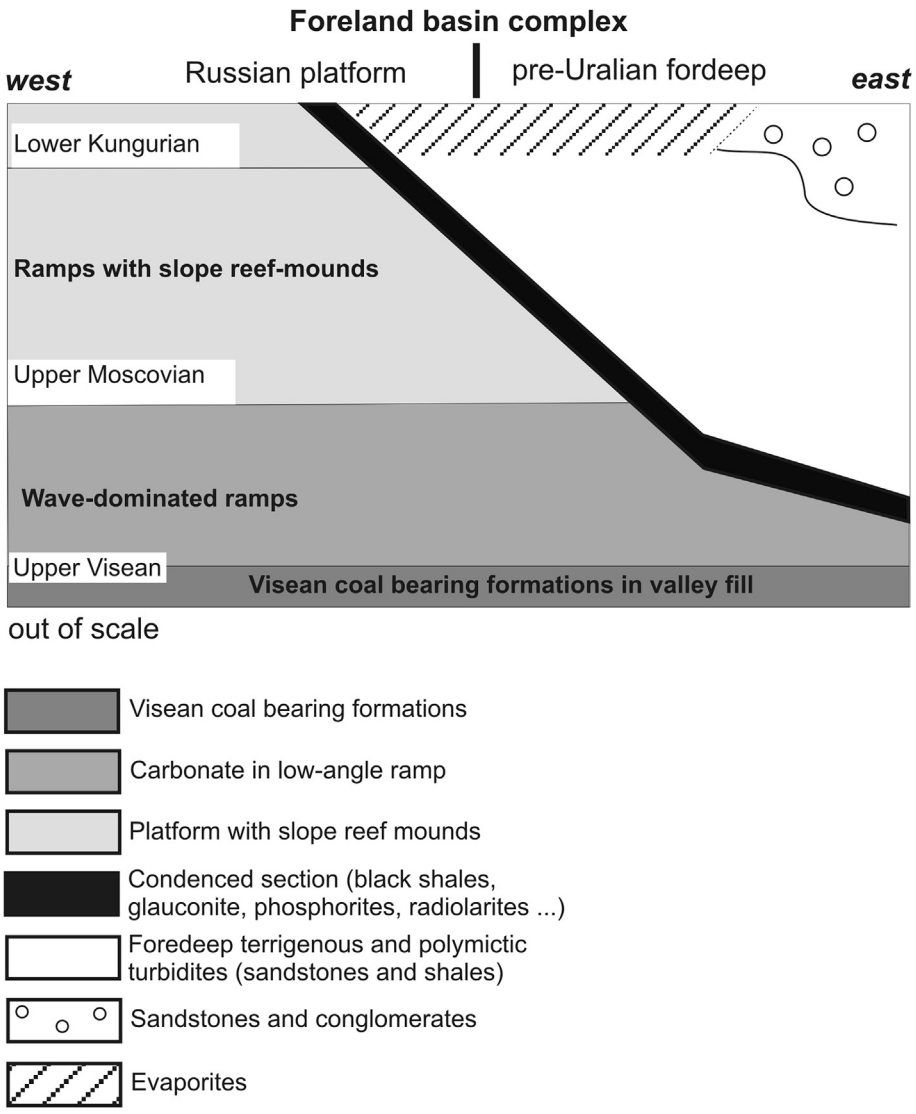

Fig. 2. Simplified scheme of the eastern border of the Russian carbonate platform forming a ramp-like morphology to the east towards the Pre-Uralian fore deep characterized by terrigenous turbidites. The carbonate deposits rest upon Visean terrigenous, coal bearing valley infills. Through time, the mid-Carboniferous carbonate ramp changes into a carbonate platform with a well-defined slope buried by evaporites during the early Kungurian (modified after Proust et al., 1998).

averaged internal standard deviations and the averaged difference of all duplicates suggests a variability of 0.08‰ for carbon and 0.09‰ for oxygen in all samples. Values are expressed in ‰ with respect to the Vienna PDB (V-PDB) standard.

4.2. Cathodoluminescence and fluorescence microscopy

Cathodoluminescence (CL) microscopy examination of different paragenetic phases termed Ca-1 through 5 was performed to obtain qualitative information on the geochemistry and precipitation environment of these fabrics. This was carried out with the 'hot cathode' CL microscope (type HC1-LM) at the Ruhr-University Bochum, Germany. The acceleration voltage of the electron beam is 14 kV and the beam current is set to a level gaining a current density of ~9 μA mm-2 on the sample surface. Refer to Christ et al. (2012) for details on the analytical procedure. Fluorescence (FL) microscopy of hydrocarbon inclusions was performed using a Leica EL6000 instrument using a mercury short-arc reflector lamp.

4.3. Porosity and permeability analysis

The determination of porosity and permeability values was performed on the UltraPoroPerm-500 installation in the uniform integrated module at the Kazan Federal University, Russia. Prior to analysis, full-size core cylinders of 30x50 mm were drilled out of samples. Hydrocarbons were extracted prior to analysis using the method described in Gordadze and Tikhomirov (2005). Pore space of samples was cleaned from oil, bitumen and also (non-diagenetic) salts (extraction). The solvents used included chloroform or ethanol and benzene mixed in a ratio of 1:1. The sample was placed in a cell equipped with a sample holder. A helium gazo-broad porozimeter with a high-precision linear converter of excessive pressure of 0–250 psi (0–17 bars) with a hysteresis less than ±0.11% of a limit of measurements was used. Permeability was measured on nitrogen gas with an atmospheric pressure. The measured porosity range is expressed as 0–40 units of porosity whilst the measured permeability range is expressed as $0.01 \cdot 10^{-3}$ μm^2 to $15 \cdot 10^{-3}$ μm^2.

X-ray tomography investigations were conducted using an industrial x-ray microtomography, Phoenix V|tome|X S 240 (Carl

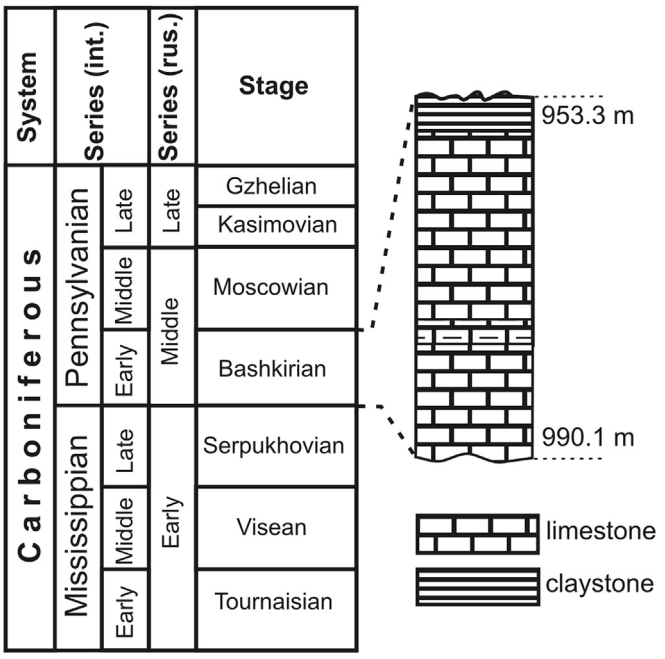

Fig. 3. Stratigraphy and general lithology of Bashkirian stage in the Melekesskaya depression with indication of international and Russian stratigraphic scheme. Note depths refer to absolute depth, i.e. meters below land surface.

Zeiss) at the Kazan Federal University, Russia. The system has two x-ray tubes 1) one being microfocal with maximum accelerating tensions of 240 kV/320 W and 2) one being nanofocal with maximum accelerating tensions of 180 kV/15 W. For the pre-processing of data and the creation of a pore volume model of a sample on the basis of x-ray pictures (projections) the software datos|x reconstruction was used. For data visualization and the analysis of data on elements of the volume image the software of VG Studio MAX 2.1 and Avizo Fire 7.1 was used.

4.4. Microthermometry

Sample C-133 (taken at core meter 1284) was cut perpendicular to the orientation of the idiomorphic Ca-5 generation and prepared as double polished thick section (~200 μm). Paragenetic phases Ca-2 to 4 do not show a preferred orientation of crystal c-axes. Relative chronological sequences of fluid inclusions (fluid inclusion assemblages (FIA) after Goldstein and Reynolds, 1994) were then established and documented by optical microscopy. Clearly identified primary (p), pseudo-secondary (ps) and secondary (s) inclusions were identified. A detailed explanation of fluid petrography terminology is given in Walter et al. (2015, their Fig. 4).

Microthermometric investigations were elaborated using a Linkam (model THMS 600) heating-freezing stage on a Leica DMLP microscope at fluid laboratory at Tübingen University. For each inclusion, we measured the final melting temperature of ice ($T_{m,ice}$), the final hydrohalite dissolution temperature ($T_{m,hh}$), and the homogenization temperature (T_h). For calibration, synthetic H_2O, H_2O–NaCl, and H_2O–CO_2 standards were used and only results with a maximum admissible variation of the final melting temperatures of less than 0.1 °C were used for data interpretation. For homogenization temperatures, a maximum admissible variation of up to 1 °C was accepted due to poor visibility in some samples. A limited number of inclusions and measurements with outlier in salinity and homogenization temperature within a homogeneous trail were disregarded as post-entrapment modification cannot strictly be excluded.

For the calculation of salinity and Ca/(Na + Ca) mole ratios, the Microsoft Excel-based calculation sheet of Steele-MacInnes et al. (2011) for the ternary NaCl–$CaCl_2$–H_2O system was used. The degree of fill was assessed optically with filling degree tables and illustrations of Shepherd et al. (1985). Pressure correction was done using the formula of Bodnar and Vityk (1994) in combination with estimates on sedimentary overburden based on Fig. 1.

5. Results

5.1. Gamma ray and electrical log, porosity, permeability, and oil saturation

Facies patterns data agree well with the gamma ray log data shown in Fig. 5. Essentially, the Bashkirian interval is built by a clean carbonate succession overlain by Moscovian clays. Electrical log data do not cover the full oil-water transition zone but terminate at the oil-water contact (sub-interval II).

The distribution of pore space is irregular both in the oil-saturated productive zone and across the oil-water transition interval (Fig. 5; Table 1). In the oil-saturated zones of the lowermost productive zone, i.e., the top of the core interval studied here, the dominant pore type is intergrain porosity (mean value of total (helium) porosity = 14%). Further down core into the oil-water transition zone intergrain porosity is still recorded but we also observe large cavernous pores and leaching along fractures. At the upper portions of the oil-water transition interval, mean measured values suggested 7–8% porosity whilst at the base of the core, i.e. the lower portion of the oil-water transition zone, porosity values of between 22 and 24% were found and permeability increases rapidly (Fig. 5, Table 1). The down core increase in porosity is well correlated with the increase of large cavernous pore space. Permeability data reveal a very similar overall pattern with values being very low and invariant at the base of the productive zone and across most of the oil-water transition zone (Fig. 5). Please refer to Table 1 for details. Centimetre-sized cavernous pores often connect through nets of leached channels. A prominent case example was studied by means of x-ray tomography and is documented in Fig. 6.

Oil-saturation was determined qualitatively from direct core observation. Oil-saturation is spatially irregular and decreases down core from the reservoir zone towards the water saturated zone. Within the base of the productive zone, limestone intervals with a high degree of oil saturation alternate with such that contain only limited volumes of hydrocarbons in pore space. The aquifer below the oil-water transition zone was not cored.

5.2. Petrography, mineralogy, and cathodoluminescence properties of carbonate cements

Based on rock sample (Figs. 4 and 7 through 9), thin section and cathodoluminescence analysis, the following petrographic succession has been established: (i) Phase Ca-1 (Fig. 10) representing the host sediment is characterized by differential degrees of diagenetic alteration. Very localized, early marine cements are present. This early marine fibrous phase nucleates on recrystallized coral skeletons (Fig. 4E, F) but is not considered any further here due to its volumetrically subordinate nature. The host sediment is commonly orange luminescent. The Ca-1 host sediment substratum is overlain by a non-luminescent early diagenetic, blocky to stubby calcite phase (50–500 μm in thickness) often, but not always, characterized by one to up to ten thin orange to yellow luminescence subzones in its outer portions (Ca-2; Figs. 8 and 9). Ca-2 cement morphologies are euhedral to anhedral depending on the morphology of the pore space they occlude. Phase Ca-2 is common

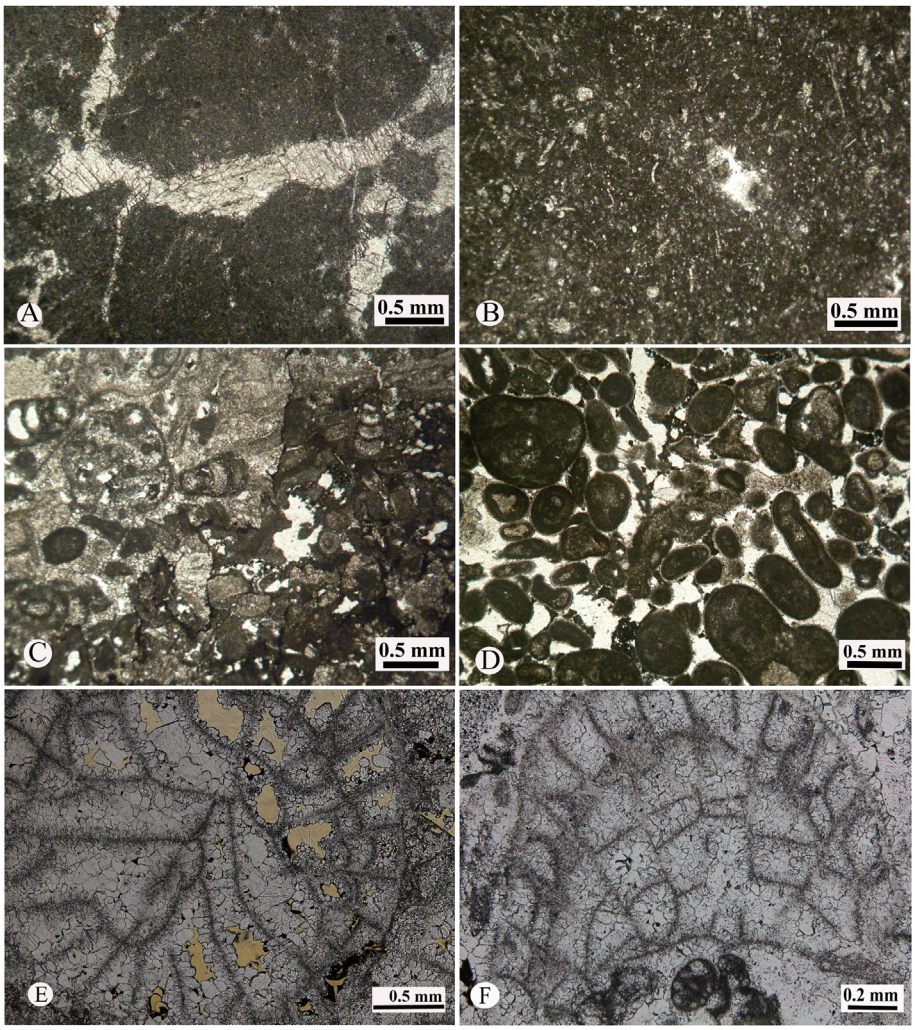

Fig. 4. Thin section images characterizing the different facies types present in the oil-water transition interval studied. (A) Peloidal mudstone with late diagenetic fractures filled by blocky calcite. (B) Fine-grained, argillaceous wackestone with abundant unspecified skeletal debris. (C) Coarse-grained algal, foraminiferal packstone. (D) Oncoidal and ooidal grainstone with composite grains and superficial ooids. (E/F) Coral framestone, note blocky calcite filling recrystallized coral skeletons. Early marine cement phase forms thin, isopachous rim on coral skeletons.

in all Bashkirian samples.

The next diagenetic phase paragenetically (Ca-3) is a dull to bright luminescent, usually blocky calcite (Figs. 8 and 9) with dimensions of some tens to some hundreds of μm depending on the size of the pore space occluded. Luminescence patterns reveal a complex zonation and banding in places. Often the luminescence color changes from bright to darker orange towards the crystal margins. The surfaces of Ca-3 calcite cements are commonly corroded and irregular (Fig. 8B, F). Ca-3 calcites are overlain by a volumetrically insignificant dolomite phase (Dol in Fig. 9F) characterized by a red, mottled luminescence color. Dolomite crystals usually are present as single crystals or as cluster of crystals each with a corroded surface (Fig. 10E and F). In some cases, relictic rhomboedric shapes of dolomite crystals are preserved.

The next fabric is stratigraphically represented by coarse blocky crystals of calcite (Ca-4) and forms one of the volumetrically most significant phases (some hundred μm to 1 cm in diameter; Fig. 7 through 9). Phase Ca-4 has a dark red or dark brown luminescence color often with a darker or lighter brown luminescence zone at its outer crystal margins. Two subtypes are observed. Subtype Ca-4a is a translucent blocky cement phase, whilst subtype Ca-4b is translucent but porous and yields numerous hydrocarbon inclusions ranging in size up to some tens of μm (Fig. 8D). Commonly, the surfaces of calcite phase Ca-4b are corroded (Fig. 8D, F). Subtypes 4a and 4b coexist in some samples. In this case, phase 4b overlies 4a with a sharp and planar boundary (Fig. 8D). Elsewhere, only subphase 4a (Figs. 8B and 9F) or subphase 4b (Fig. 8F) are present.

The paragenetically youngest, often blocky cement phase (Ca-5) is alternating light or dark orange under the cathodoluminescence and displays complex sectorial zoning (Fig. 8F). Crystals are similar in size to phase 4 and reach dimensions of many 100 μm to one cm.

5.3. Microthermometry and fluorescence

Green fluorescence colors of oil inclusions in phase 4 cements were found to be of limited diversity all thin sections studied. Non-oil fluid inclusions were recognized in paragenetic stages 3 through 5 and are document in Figs. 10 and 11. In phase 3 calcites, only liquid monophase fluid inclusions were observed. For calcite generations 4 and 5 detailed microthermometric investigations were performed. Freezing temperatures vary between −70 and −100 °C. First melt can be determined around −50 °C that implies a eutectic at −52 °C that is related to the ternary H_2O–NaCl–$CaCl_2$ system.

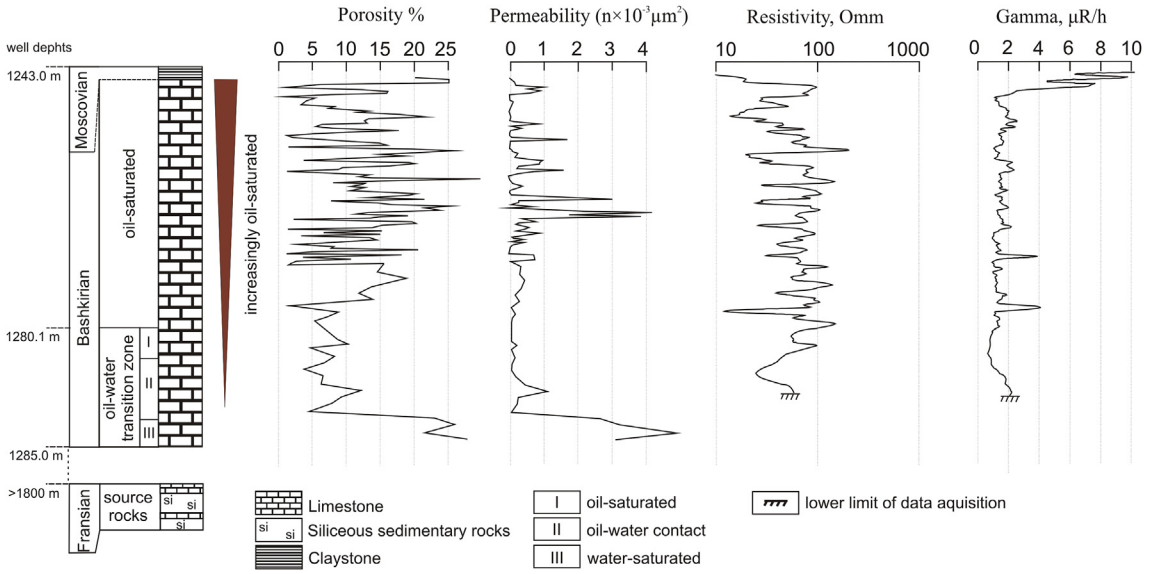

Fig. 5. Schematic geological section of reservoir facies and oil-water transition zone with indication of porosity, permeability, resistivity, and gamma ray data. Transition zone is indicated and subdivided in sub-zones I through III, with I being located at the limit to the overlying productive zone and III at the limit to the underlying water-wet zone. Note, depths are well depths in meters.

Table 1
Porosity-permeability data and type of porosity across the oil-water transition zone.

Zones	Depth, m	Value of open pore space, %	Permeability by gas (n × 10^{-3} μm^2) across layers succession	Type of porosity
Lower part of oil reservoir				
Oil-saturated	1276.5	15.57	0.29	intergrain
	1276.9	14.68	0.27	
	1277.2	18.77	0.40	
	1277.6	13.69	0.30	
	1277.9	12.01	0.12	
	1278.2	13.88	0.24	
	1278.5	2.17	0.01	
	1278.8	8.98	0.11	
	1279	7.47	0.04	
	1279.2	5.69	0.00	
Oil-water contact				
I	1280.1	8.88	0.01	intergrain
	1280.3	10.18	0.16	
	1280.5	5.13	0.01	
	1280.9	8.49	0.10	
	1281.2	7.2	0.03	
	1281.5	4.27	0.01	
	1281.8	6.78	0.13	intergrain and solution-enlarged
II	1282.2	6.52	0.42	
	1282.5	12.15	1.06	
	1282.8	9.56	0.20	
	1283.1	8.06	0.18	
	1283.5	4.78	0.01	
	1283.8	22.75	2.63	cavernous
III	1284.1	25.64	3.21	
	1284.5	21.32	4.89	
	1284.8	27.50	3.10	

Degree of fill shows constant values between 0.9 and 0.95.

For calcite 4, final melting temperature of ice varies from −18.3 to −20.7 °C and final dissolution temperatures for hydrohalite between −22.9 and −24.1 °C, that records a salinity of 20.7–22.2 wt.% (NaCl + $CaCl_2$). Homogenization temperatures vary from 107 to 140 °C (Fig. 10). The molar Ca/(Na + Ca) ranges between 0.13 and 0.21. Based on the ternary system a Ca content of 17000–27000 ppm and a Na content of 55000–67000 ppm can be calculated. Within one single trail, salinity and T_h are almost constant whilst these values vary between different trails.

In contrast for Ca-5 the microthermometric results for the final melting of ice show a variation from −18.8 to −21.9 °C and final dissolution temperatures for hydrohalite in the range of −24.8 and −29.6 °C (Fig. 11). These measurements can be translated into salinities of 20.8–22.7 wt.% (NaCl + $CaCl_2$). The molar Ca/(Na + Ca) ratio show in average a significant higher Ca content in the fluid from 0.26 to 0.53 with a calculated Ca content of 31000–53000 ppm and Na content of 27000–50000 ppm. Homogenization temperatures are in average lower as for Ca-4 and range from 80 to 118 °C (Fig. 10).

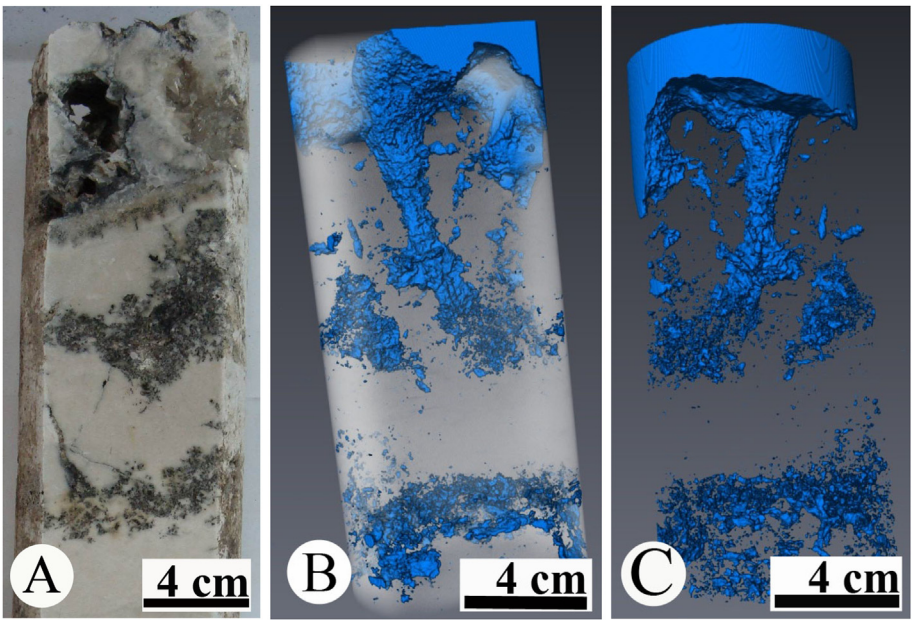

Fig. 6. X-ray tomography of core sample 1284.3–1284.6 m from sub-zone III close to the underlying water-filled interval. A) Photograph of core sample. B) Distribution of pore space in sample (blue). C) Display of pore space. Note cm-sized, spatially connected (cavernous) porosity (For interpretation of the references to color in this figure legend, the reader is referred to the web version of this article.).

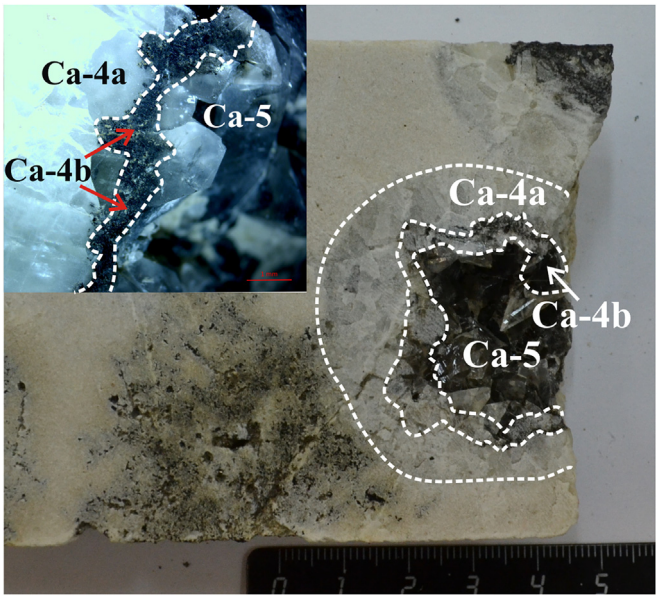

Fig. 7. Core sample and position of selected types of calcite cements Ca-4a, 4b and 5 that represent the volumetrically most important phases. Note black staining by hydrocarbons. Diameter of small upper left inset is 1.5 cm (For interpretation of the references to color in this figure legend, the reader is referred to the web version of this article.).

5.4. Carbon and oxygen isotope data of bulk micrites and carbonate cements

Bulk micrite $\delta^{13}C$ data range from −6.4 to −3.4‰ (n = 16; mean = −5.0‰) whilst $\delta^{18}O$ ratios are between −6.7 and −5.7‰ (n = 16; mean = −6.2‰; Table 2). Essentially, carbon isotope values shift to more negative values from the oil-water contact zone (~-4‰) upcore into the oil saturated zone (~−6‰). Conversely, oxygen isotope data remain comparable invariant across the short core section measured (Fig. 12).

Carbonate cement subsamples were collected from phases Ca-4a, Ca-4b and Ca-5, as these fabrics are volumetrically large enough to allow for the mechanical extraction of sample powder (Fig. 15; Table 3). The scatter of data is significant and ranges from −22.2 to −4.5‰ for carbon and from −6.7 to −4.9‰ for oxygen (Table 3). From carbonate phases Ca-2 and Ca-3, only one bulk sample could be extracted and the resulting values are −4.5‰ for carbon and −6.7‰ for oxygen. The significance of this small data set is unclear. Conversely, data from cement phases Ca-4a and b and Ca-5 are considered significant (Fig. 13). Generally, stage 4 and 5 cements are conspicuously depleted in $\delta^{13}C$ relative to the paragenetically earlier cement phases Ca-2 and 3 and bulk micrite samples, whilst they are similar in their oxygen isotope ratios. Carbon isotope data for Ca-4a cement range between −22.2 and −19.7‰ (n = 4) and represent, with respect to $\delta^{13}C$ the isotopically most depleted cluster in carbon-versus-oxygen isotope cross-plots. Oxygen isotope data of phase Ca-4a range from −4.9 to −5.4‰ (n = 4). Phase Ca-4b is slightly less depleted (−18.3‰), in ^{13}C relative to phase Ca-4a whilst $\delta^{18}O$ ratios are similar (Fig. 13). The paragenetic youngest (Ca-5) cement phase yields $\delta^{13}C$ ratios of between −12.6 and −11.2‰ (n = 3), $\delta^{18}O$ ratios are between −5.4 and −5.1‰ (n = 4) and plot in a specific cluster that is intermediate between bulk micrite and phase Ca-4 samples.

6. Interpretation and discussion

6.1. Cementation dynamics and timing of oil charge

Three subzones are subdivided across the transition zone: Subzone I represents the stratigraphically highest interval (1280.1–1281.8 m) directly beneath the productive, fully oil-saturated zone of the reservoir (Figs. 5 and 12). Subzone III is located in the lower part of oil-water transition zone (1284.1–1284.8 m), i.e. directly above the water-wet zone where oil-filled pores are rare to absent. Subzone II is intermediate in nature (Figs. 5 and 12). This subdivision is - to some degree –

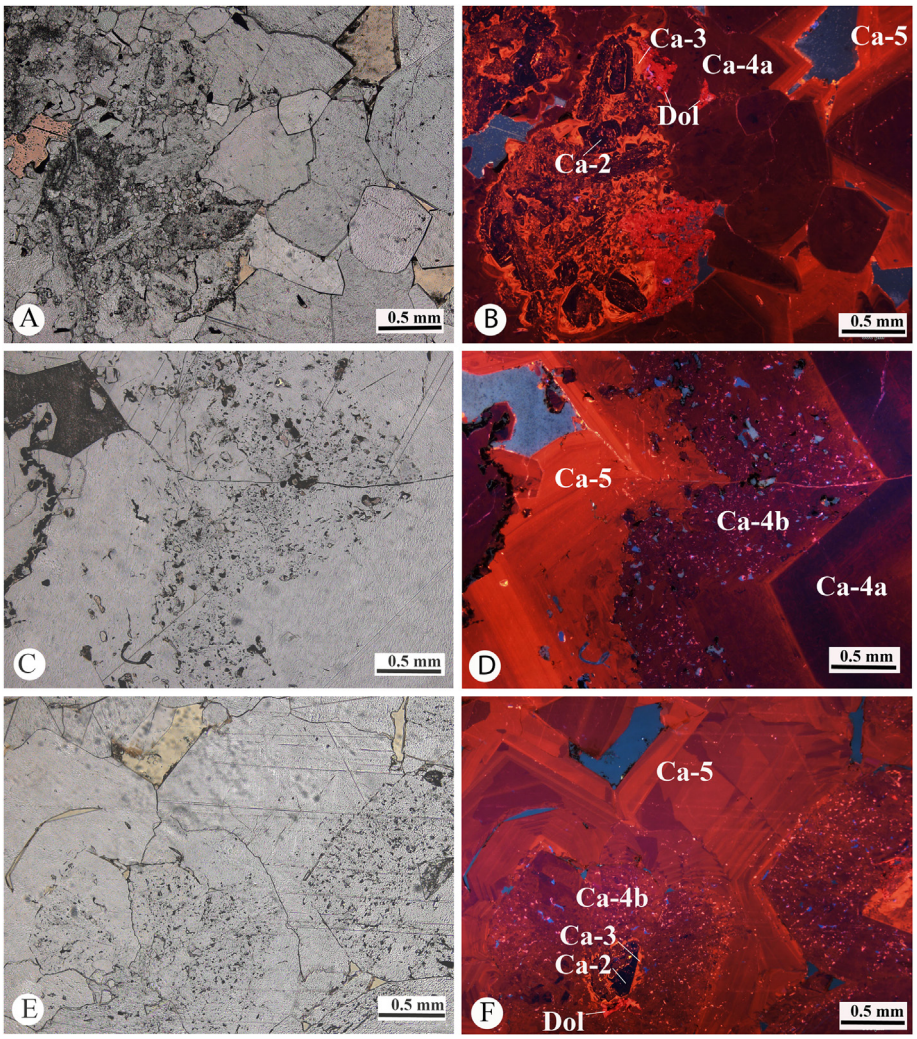

Fig. 8. Cathodoluminescence properties of different paragenetic phases placed against transmitted light photomicrographs. (A/B) Complex intergrowth of different cement types including a dolomite phase (Dol). (C/D) Cement phase Ca-4a, b and 5. Note sharp boundary between phase 4a and 4b and corrosive boundary to overlying phase Ca-5. Ca-4b is interpreted as paragenetic phase coeval to oil migration due to numerous hydrocarbon inclusions. Note complex zoning of phase Ca-5. (E/F) as (C/D), note hydrocarbon inclusions in phase Ca-4b and complex sector zoning of phase Ca-5.

artificial in nature as the boundaries are not sharp but gradual but serves the purpose to simplify the discussion.

The paragenetic succession of carbonate cements observed in thin sections from each of these subzones shares important similarities and differences (Fig. 14A–C). Paragenetic stages Ca-1, 2, and 3, representing the pre-emplacement phase, are present in all samples studied. Ca-1 represents the diagenetically stabilized sediment substratum upon which a series of marine to burial carbonate cements precipitate. The patchy luminescence of Ca-1 reflects the typical admixture of sediment consisting dominantly of magnesian calcites and probably aragonite particles that were later stabilized to diagenetic calcite in the presence of reducing fluid as evidenced by luminescence. Pore space is largely occluded by non-luminescent Ca-2 cements also found as first phase nucleating upon the sedimentary substratum (e.g., Fig. 9B and D). Following previous workers (Bruckschen and Richter, 1994), phase Ca-2 cements are here not considered fully marine in nature but probably represent a shallow burial phase (Kaufmann, 1997) precipitated from modified marine porewaters. In previous work (Walkden and Williams, 1991; Bruckschen et al., 1992; Bruckschen and Richter, 1994; Richter et al., 2003; Swart, 2015), thin yellow luminescent zones (Fig. 9D) in otherwise non-luminescent calcite cements have been interpreted as representing pulsed changes in Eh with transient intervals of sub-oxic fluids leading to the presence of Mn^{2+} incorporated into the crystal lattice (Bruckschen et al., 1992; Richter et al., 2003). Nevertheless, the oxidation stage of the pore fluid, and related to this the presence of Mn^{4+} and Mn^{2+} respectively, is not the only factor that must be considered. Based on experimental work Ten Have and Heijnen (1985), documented that differences in crystal growth rates significantly affect the luminescence patterns of carbonate cements. Moreover, activators other than Mn^{4+} (and quenchers) must be considered.

Similar to Ca-2, cement phase Ca-3 is present throughout all subzones of the water-oil-transition interval. The luminescence patterns of this phase are complicated showing banding and sector zoning (Fig. 9B and 14). In many cases, this phase is corroded at its outer margin pointing to a stage of non-cementation and corrosion between phase Ca-3 and Ca-4 most likely related to a change in pore fluid chemistry (Fig. 15). In several of the thin sections studied, phase Ca-3 is locally overlain by patchy dark-red to orange-brown luminescent, layered dolomite rhombs (Fig. 9F and 14) present throughout subzones I to III (Fig. 15). The precipitation of the dolomite spans the diagenetic stages of early hydrocarbon charge. Evidence for this comes from the inclusions rich-, corroded nature

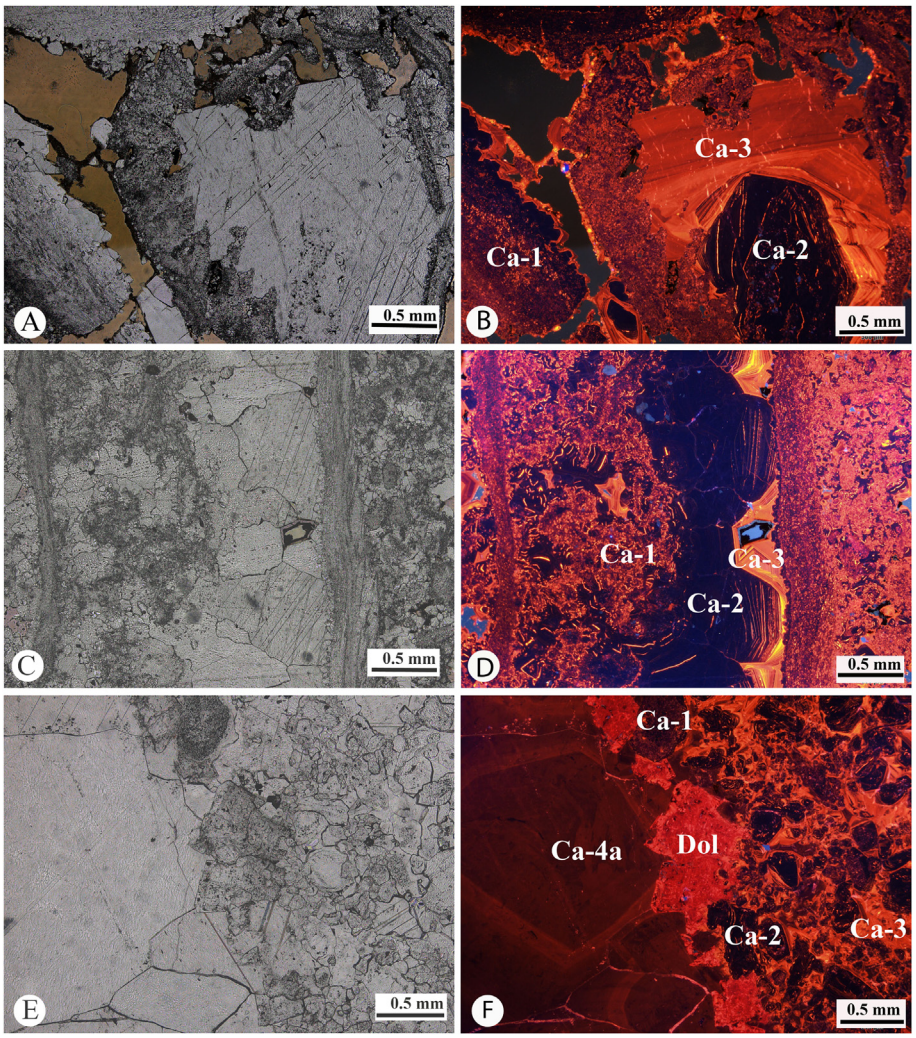

Fig. 9. Cathodoluminescence properties of different paragenetic phases placed against transmitted light photomicrographs. (A/B) Host sediment (Ca-1), non-luminescent blocky spar calcite (Ca-2), and bright orange luminescent blocky spar calcite cement (Ca-3). Note complex zoning of Ca-3. (C/D) Phase Ca-2 and 3 overlaying sediment substratum. Note bright luminescent zones in otherwise non-luminescent Ca-2 phase cements. (E/F) Coarse blocky Ca-4a phase overlying patchy luminescent dolomite cements (Dol) (For interpretation of the references to color in this figure legend, the reader is referred to the web version of this article.).

of the dolomite rhombs and paragenetic position overlying phase Ca-3a calcites. Dolomite precipitation is potentially related to changes in the partial pressure of fluid CO_2 (Morrow, 1982) with the first migration fronts of fluids ahead of the rising hydrocarbons being enriched in CO_2. This notion is in agreement with cement Ca-3 corrosion (Fig. 15).

Dark brown-red luminescent cement phase Ca-4a and b are of key significance for the understanding of the oil charge history of the Bashkirian reservoir facies under study. Based on the microthermometric data compiled here, phase Ca-4a and b cements precipitated from fluids with a salinity range of between 20.7 and 22.2 wt.% (Fig. 10) and a temperature range of between 107 and 140 °C (Fig. 11). The fluid chemistry is in agreement with a non-carbonate source, i.e. the Devonian black shales representing the source rocks (Aizenshtat et al., 1998). According to basin modeling, oil migration in the Volga-Ural region started – depending to the location studied – as early as the Late Triassic and goes on until present time (Kerimov et al., 2014). Several peak intervals of oil migration and accumulation during the Mesozoic and Cenozoic were proposed. Most workers, however, agree that the main oil migration and accumulation phase correlates with an Alpine stage of a tectogenesis. Based on regional data, the Alpine orogenic stage in the Oligocene to early Pliocene (Sharkov et al., 2015) resulted in the formation of the majority of modern structures in the region and triggered most of the oil accumulation in these structures (Ashirov, 1960). Judging from the presence of two corroded internal surfaces (i.e., between phase 3 and 4 and between 4 and 5, Fig. 15) two pluses of ascending corrosive fluids are recorded. These perhaps point to two regionally important fluid migration events resulting from tectonic far-field effects ("squeegee flow", cf. Immenhauser et al., 2007). The latter one of these two events was related to oil emplacement.

In subzone III (Fig. 14C), i.e. the interval that is closest to the water-filled zone, phase Ca-4b is lacking whilst 4a (Fig. 8B and D, 9F) is present. The main difference between Ca-4a and b lies in the presence of abundant oil and bitumen inclusions within phase Ca-4b. The boundary between Ca-4a and b is sharp with luminescent colors gradually turning into brown to black colors with a transition to brown-orange luminescence at the base of phase 4b. In the view of the authors, phase Ca-4b is essentially coeval to initial oil charge from the Devonian source rock into the Bashkirian reservoir facies. Interestingly, subzone III cements of this stage lack oil and bitumen inclusions suggesting spatially localized oil migration as opposed to migration through the bulk lithology. The

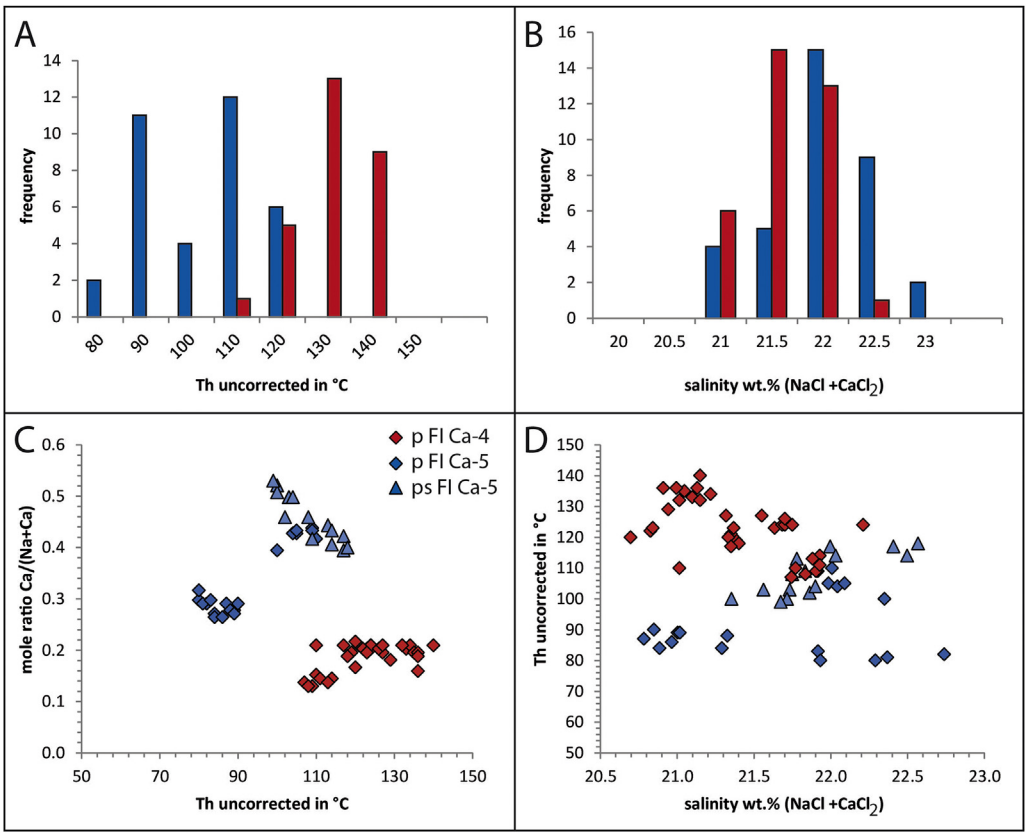

Fig. 10. Homogenization temperatures in cement phases Ca-4 and 5. (A) Histogram of measured homogenization temperatures. (B) histogram of calculated salinities in wt.% (NaCl + $CaCl_2$), (C) homogenization temperatures versus Ca/(Na + Ca) mole ratio, (D) salinity wt.% (NaCl + $CaCl_2$) versus homogenization temperatures. Note systematic variation (A–D) of fluids trapped in Ca-4 (red) and Ca-5 (blue) (For interpretation of the references to color in this figure legend, the reader is referred to the web version of this article.).

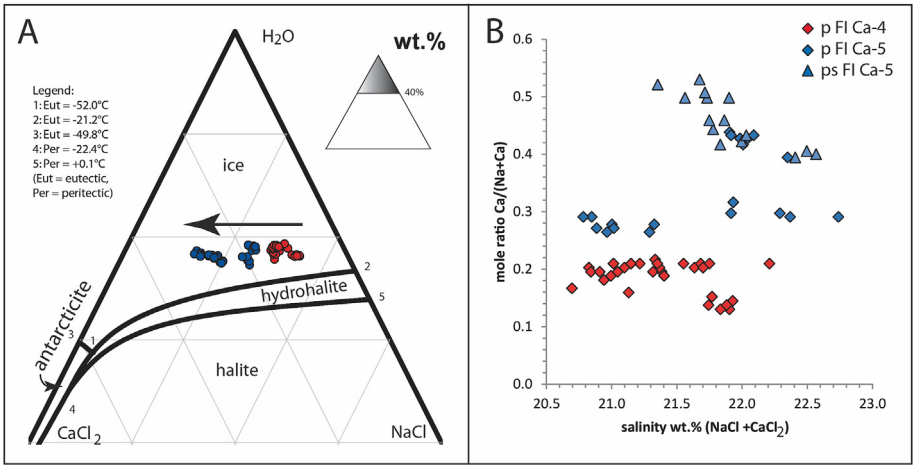

Fig. 11. Fluid salinity in cement phases Ca-4 and 5. (A) Microthermometric results in the ternary NaCl–$CaCl_2$–H_2O phase diagram. (B) salinity wt.% (NaCl + $CaCl_2$) versus Ca/(Na + Ca) mole ratio. Note systematic variation of fluids trapped in cement phases Ca-4 (red) and Ca-5 (blue) (For interpretation of the references to color in this figure legend, the reader is referred to the web version of this article.).

very limited spread of hydrocarbon inclusions fluorescence colors (green, wavelength of 548 nm) implies a single maturity of included oil (see discussion in Sellwood et al., 1993). In subzones I and II, phase Ca-4b is in turn corroded and in all subzones overlain by stage Ca-5 cements with complex luminescence banding and sector zoning (Fig. 8D, F and 14A, B). Based on microthermometric data, stage Ca-5 cements precipitated from fluids with a salinity range of 20.8–22.7 wt.% (Fig. 10), i.e. directly comparable to those of Ca-4 fluids, and a temperature range of 80 though 118 °C (Fig. 11). This fluid temperature range is lower by about 20 °C relative to Ca-5 fluids and judging from the fluid chemistry, these are mainly carbonate hostrock derived (Figs. 13 and 16). It is suggested that the initiation of phase Ca-5 cement precipitation reflects the end of the hydrocarbon migration and the post hydrocarbon stage (Fig. 15).

In comparison to previous studies linking oil charge with cement stratigraphy, the limitation of oil inclusions to one distinct

Table 2
Geochemical data of host matrix micrite bulk samples.

Subzones	Sample name	Well depth, m	$\delta^{13}C$ [‰](VPDB)	$\delta^{18}O$ [‰](VPDB)
I	L122a	1280.2	−6.1	−6.2
	L122a1	1280.3	−6.1	−6.2
	L123a	1280.5	−5.5	−6.3
	L123a	1280.5	−5.5	−6.2
	L124a	1280.7	−6.4	−5.7
	L125a	1281.1	−6.3	−6.3
	L126a	1281.5	−5.1	−5.7
	L127a	1281.8	−4.8	−6.2
II	L128a	1282.2	−4.2	−6.3
	L129a	1282.5	−4.2	−6.7
	L130a	1282.8	−4.5	−6.0
	L130a1	1283.1	−4.4	−6.2
	L132a	1283.5	−4.3	−6.1
	L133a	1283.8	−3.4	−6.2
III	L135a	1284.2	−4.0	−6.4
	L136a	1284.8	−4.3	−6.1

subzone III through I, i.e. towards the oil-saturated zone. It seems likely that this pattern reflects the presence of oil-derived light organic carbon included in the crystal lattice of inorganic calcite phases.

All bulk sediment and cement values are depleted in both ^{13}C (−4 to −23‰) and ^{18}O (−4.7 to −6.7‰) relative to reconstructed marine seawater values for the Bashkirian. Grossman et al. (2002) report Bashkirian brachiopod shell data from the Russian platform and find $\delta^{13}C$ values in the order of +5‰ and $\delta^{18}O$ in the order of −1.5‰. Particularly, the difference of about 10‰ in carbon isotope ratios between reconstructed seawater DIC (+5‰) and measured bulk micrite data (−5‰) is remarkable (Fig. 13). Essentially, phase Ca-2 and 3 plot in the same range in terms of carbon isotope ratios but are more ^{18}O-depleted relative to bulk sediments and other phases. In the absence of evidence for meteoric diagenesis, this may imply dissolution and reprecipitation processes of a formerly shallow marine burial phase in the presence of warm pore

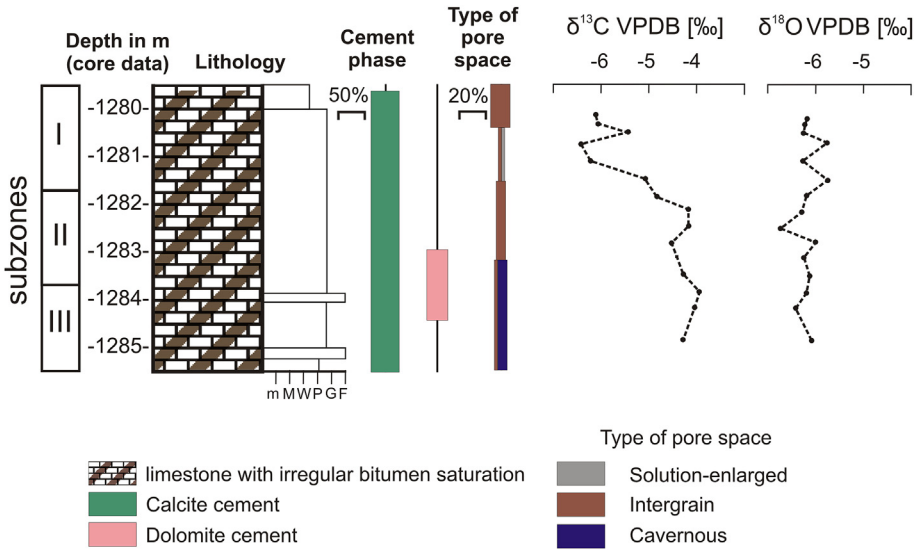

Fig. 12. Detailed geological section across oil-water transition zone with geochemical data, cement types and porosity. Note gradual depletion in ^{13}C from sub-interval III through I. Note, depths are well depths in meters.

paragenetic stage is uncommon (Simo and Lehmann, 2000). From a Cretaceous carbonate field in the U.A.E., Cox et al. (2010) for example, describe not less than 12 subsequent cathodoluminescence zones with oil inclusions. The later notion is in concert with oil charge and cement growth occurring synchronously over very extended time periods. Judging from the data shown here, the Bashkirian oil leg was charged rapidly and perhaps during a comparably brief period triggered by alpine tectonism (Fig. 15 through 17). Having said that, it is conceivable that the corroded surface between phase 4b and 5 (e.g., Fig. 8D) represents a cementation hiatus of unknown duration.

6.2. Carbonate isotope evidence

Carbon and oxygen isotope analyses were obtained from bulk sediments (mainly the fine grained micritic phase; Table 2) as well as from cement phases Ca-4 and 5 (Table 3). Cement volumes of phases Ca-2 and 3 are too small to mechanically separate phase-specific powder samples and hence, these phases were lumped in one analysis. Bulk matrix micrite values are plotted stratigraphically across the palaeo-oil-water transition zone (Fig. 12) and reveal a clear trend to increasingly ^{13}C-depleted values from fluids with a near-marine salinity. In comparison to published $\delta^{18}O$ values of calcite cements in some carbonate reservoirs (~−10 to −14‰; Cox et al., 2010), however, the oxygen isotope values shown here are not remarkably depleted. Using temperature equations for calcite $\delta^{18}O$ (Kim and O'Neil, 1997), a lower formation water temperature limit of 45 °C can be extrapolated but this depends on the choice of the $\delta^{18}O_{fluid}$ and the unknown fluid salinity and must be accepted within geologically reasonable error bars (Fig. 13).

Cement stages Ca 4a and b as well as 5 are less depleted in ^{18}O relative to bulk sediments and altered, early stage cements Ca-2 and 3 whilst they are more depleted in carbon isotope ratios (Fig. 13). The decreasing cement $\delta^{13}C$ with increasing burial depth contrasted by moderately increasing $\delta^{18}O$ is uncommon (Cox et al., 2010). In the view of the authors, slightly less ^{18}O depleted values of cement phases 4 and 5 might either imply a decrease of formation water temperature or, perhaps more likely, an increase of fluid salinity or a combination of both (Steinhauff et al., 1999). The opposing trend, i.e. increasingly ^{13}C depleted values with progressing cementation (Figs. 12, 13 and 16) is perhaps best explained in the context of volumetrically significance volumes of ^{13}C depleted organic matter related to hydrocarbon migration.

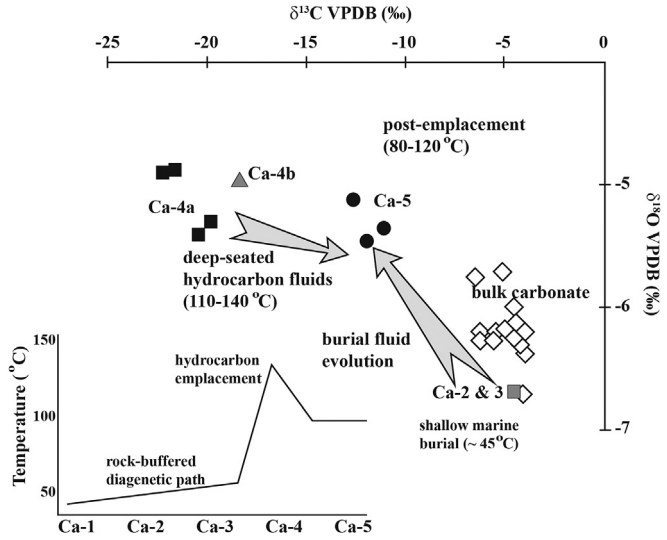

Fig. 13. Cross plot of carbon and oxygen isotope values measured from bulk sediment part of samples and different types of calcite cements with indication of reconstructed fluid palaeotemperature. Note trend to more depleted ^{13}C values of cement phases Ca-4 and 5 relative to bulk sediment. Lower left inset displays schematic temperature history of paragenetic phase Ca-1 through Ca-5. See text for discussion.

Particularly, the most depleted phase 4a is characterized by numerous oil inclusions suggesting that these cements grew in pores that contained both water and oil. It seems likely that organic compounds released ^{13}C-depleted carbon in the precipitating fluid that was then included in the calcite lattice. In agreement with the interpretation brought forward, oil charge took place during the Ca-4a cementation stage and consequently, carbon isotope values of this phase are the most depleted ones. Source rock-derived CO_2 (~−25‰) most likely mixes with rock-derived marine carbon and the resulting data obtained from these carbonate cements precipitated from these fluids lie somewhere on a mixing line between these end members (Fig. 13).

6.3. Porosity and permeability patterns across the oil-water transition

The boundary between subzones II and III, i.e. the transition to the lower portion of the palaeo-oil-water transition zone (Fig. 5) is characterized by a marked increase in porosity from between 5 and 10% to on average 15% (peak values of 25%, Figs. 5 and 17) and permeability. Given that the carbonate facies above the oil-water transition zone is in essence directly comparable to that below, the increase in porosity and permeability is best explained by the differential diagenetic history of the productive zone relative to the oil-water transition interval. Judging from the data available, the syn-oil emplacement phase Ca-4b and particularly the post emplacement phase Ca-5, that occludes significant portion of pore space in subzone I and II of the oil-water transition zone (Fig. 7), is absent in the productive zone above and the water-filled zone beneath explaining the significant increase in porosity and permeability (Fig. 5).

Judging from thin sections and particularly X-ray tomography, the general trend of increasing porosity and permeability in subzone III of the oil-water transition zone is caused by leached channels and a system of connected cavernous porosity (Fig. 6). These channels and cavernous pores are considered the result of non-equilibrium processes in the water filled zone of the transition zone, where hydrocarbons create local changes in the fluid physic–chemical properties with lowered fluid pH and a changing CO_2 regime (Helgeson et al., 1993).

6.4. Did oil emplacement inhibit carbonate cementation?

With regard to carbonate reservoirs, the commonly held view is that calcite cementation in oil saturated carbonate reservoirs is limited or inhibited in the presence of hydrocarbons, displacing burial brines. This is because the transport of dissolved ions and aquo-complexes to the site of, and required for, carbonate cementation demands an aqueous medium, usually burial brines. Cements such as dolomite, kaolinite, quartz, barite, celestine, sphalerite, and galena (Neilson and Oxtoby, 2008) form in the presence of abundant hydrocarbons in the reservoir above the oil-water contact, whereas carbonate cements precipitate in the aquifer below (Heasley et al., 2000; Worden and Heasley, 2000). These concepts can be tested using the data set presented here.

Cement phase 4b is a clear case example of a calcite phase precipitating from pore fluids containing both oil and water (Fig. 8D). Evidence comes from the numerous oil inclusions implying an initial overlap in the timing of oil migration and emplacement and phase 4b cementation. Carbonate fields are, in many cases, only weakly oil-wet (but more often mixed-wet) when compared to clastic reservoirs (Heasley et al., 2000). Essentially, oil films form at the surface of pores and adhere to carbonate surfaces whilst the bulk pore space remains water filled (mixed-wet). Moreover, oil may be transported as micro-droplets (emulsion) in essentially water-wet reservoirs and droplet were attached to the crystallization front to become subsequently built into phase Ca-4b cements. Judging from thin sections, the increasingly inclusion-rich, porous, and corroded nature of these calcites is indicative that the oil-water ratio increased and cementation was gradually retarded. At some stage, cementation ceased (Fig. 15). During peak oil migration, corrosion of carbonate cements took place leading to the formation of a hiatal interval expressed as the irregular interface between phase Ca 4b and phase Ca-5 cements. The subsequent onset of phase 5 is indicative of a significantly decreased oil-water ratio, resulted in cementation fronts that were essentially water wet, and continued cement precipitation (Fig. 15).

The data shown here for a limestone reservoir agree well with the conclusions previously drawn for quartz cementation during oil emplacement (Worden et al., 1998, 1999). These authors suggest that quartz cementation came to a halt when the precipitating fluids were unable to reach the pore space in an oil-wet system. Concluding from the here documented case example, the “oil-does-not-inhibits-diagenesis” model applies as long as the oil-to-water ratio is low. When a threshold limit is passed, the “oil-inhibits-diagenesis” model reasonably describes the formation of a corroded, hiatal surface in the cement succession occluding pore space.

7. Conclusions

(1) A detailed geochemical, cathodoluminescence, fluorescence, and microthermometric analysis of a 5-m-thick palaeo-oil-water transition zone was performed with focus on five calcite (Ca-1 through Ca-5) and one dolomite paragenetic cement phase. Diagenetic environments range from syn-depositional marine to late burial in nature.

(2) The presence of a corrosive micro-hiatal surfaces and numerous oil inclusions in phase Ca-4b cements points to ascending hot fluids with temperatures of 110–140 °C and a salinity range of 20.7–22.2 wt.% related to oil emplacement. Florescence imaging implies a single maturity of included oil. The fluid chemistry is in agreement with a non-carbonate

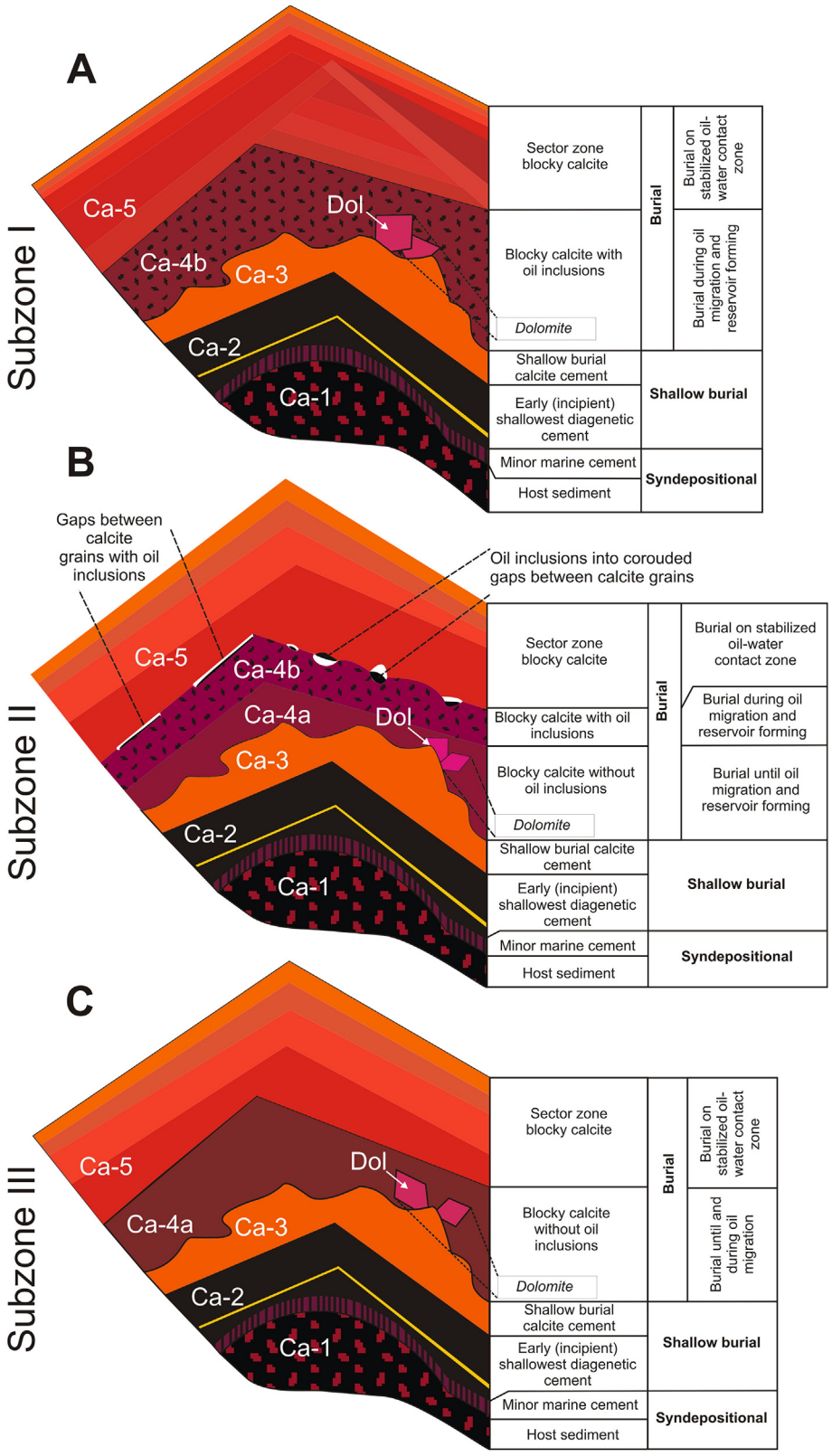

Fig. 14. (A–C). Schematic overview of cement paragenesis in subzones I (A), II (B) and III (C) of oil-water transition zone. See Fig. 12 for relative position of subzones.

source, i.e. the Devonian black shales representing the source rocks.

(3) An earlier corrosive interval, separating stage Ca-3 and 4 and cements lacking hydrocarbon inclusions is best assigned to a first pulse of ascending fluids in advance of the hydrocarbon migration front. Post oil-emplacement cements (Ca-5) reflect cooler fluid temperatures in the order of 80–120 °C and

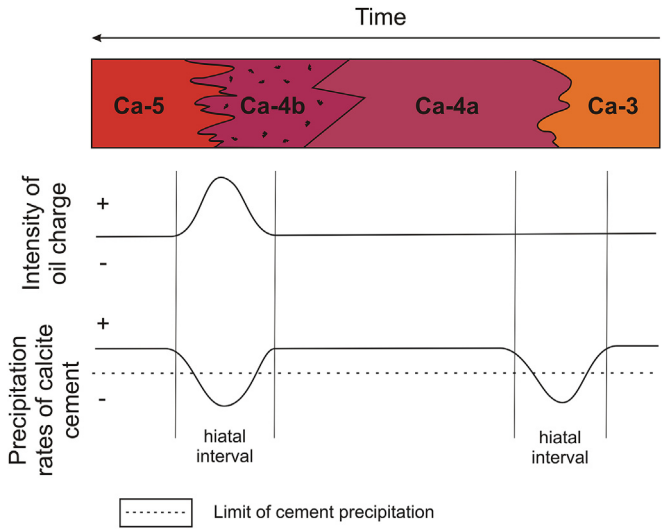

Fig. 15. Conceptual figure placing paragenetic phases versus non-precipitation/leaching leading to formation of micro-hiatal intervals in context to oil charge. Two pluses of ascending corrosive fluids are recorded in micro-hiatal surfaces. Oil charge is related to the second of these corrosive intervals. Note thickness of paragenetic phases is not to scale.

Table 3
Geochemical data of different paragenetic phases.

Sample name	Type of cement	$\delta^{13}C$ [‰](VPDB)	$\delta^{18}O$ [‰](VPDB)
C 130 a	Ca-2 & Ca-3	−4.5	−6.7
C 133 b	Ca-4a	−19.7	−5.3
C 133 d	Ca-4a	−22.2	−4.9
C 133 d	Ca-4a	−21.7	−4.9
C 136 b	Ca-4a	−20.4	−5.4
C 133 c	Ca-4b	−18.3	−5.0
C 135 a	Ca-5	−12.0	−5.4
C 136 a	Ca-5	−11.2	−5.4
C 133 a	Ca-5	−12.6	−5.1

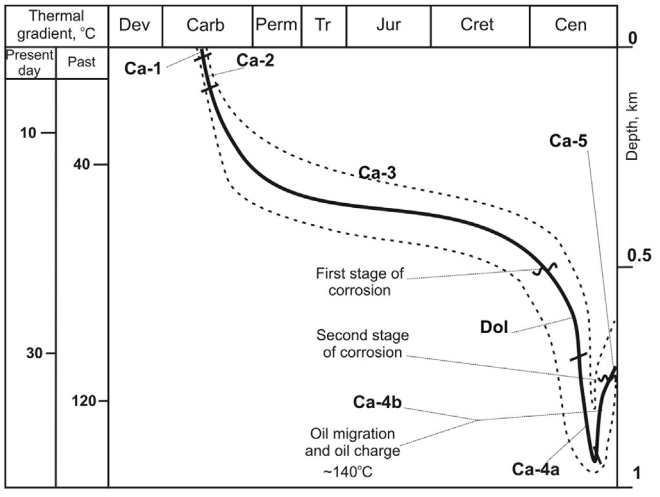

Fig. 16. Schematic temperature–time plot of basin evolution and main paragenetic events recorded in the Bashkirian carbonate rocks studied here. Note, present-day thermal gradients (measured directly in bore holes) differ from those reconstructed for Cenozoic times characterized by pulses of hot ascending fluids triggered by tectonic far-field effects. Assignment of specific paragenetic phases to specific stratigraphic intervals is not well constrained.

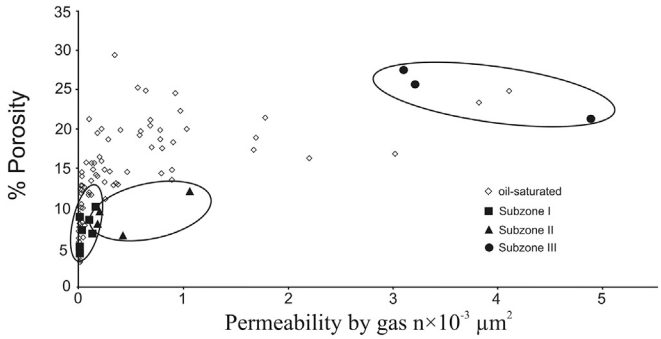

Fig. 17. Cross plot of porosity and permeability measured from oil-saturated core intervals and subzones I, II, III of oil water transition zone.

present day borehole measurements indicate temperatures in the order of about 30 °C.

(4) Porosity and permeability values are highly variable in the productive zone above the oil-water-transition zone but decrease down-core into the transition zone and increase again (up to 25% porosity) towards to water-saturated zoned. Judging from X-ray tomography, the increase in both porosity and permeability at the base of the oil-water transition zone is related to a system of leached channels and a system of connected cavernous porosity.

(5) At an early stage of oil emplacement, hydrocarbons were – in the view of the authors – transported as droplets (emulsion) in essentially water-filled pores and droplets attached to the crystallization front were subsequently built into phase Ca-4b cements. The data shown here support the "oil-inhibits-diagenesis" model but also document that cementation goes on as long as the oil-to-water ratio in mixed wet carbonate reservoirs is below an as yet undefined threshold limit.

Acknowledgments

The authors thank Dr. R. Neuser, Dr. A. Niedermayr and Dr. D. Buhl from the department of Sediment and Isotope Geology, Ruhr University, Bochum, Germany and Dr. E. Korolev from the Kazan Federal University, Russia for technical and scientific support. We acknowledge the experts reviews of K. Hollis and R.H. Worden and the editorial guidance of D.S. Alessi. This study was performed in the context of the Russian Government Program of Competitive Growth of Kazan Federal University.

References

Aizenshtat, Z., Feinstein, S., Miloslavski, I., Yakubson, Z., Yakubson, C.I., 1998. Oil-oil correlation and potential source rocks for oils in paleozoic reservoir rocks in the tataria and perm basins, Russia. Org. Geochem 29, 701–712.

Al-Dhahli, A., Geiger, S., van Dijke, M.I.J., 2014. Impact of pore-scale three-phase flow for arbitrary wettability on reservoir-scale oil recovery. J. Pet. Sci. Eng. 121, 110–121.

Alekseev, A.S., Kononova, L.I., Nikishin, A.M., 1996. The devonian and carboniferous of the Moscow syneclise (Russian platform): stratigraphy and sea-level changes. Tectonophysics 268, 149–168.

Ali, M.Y., 1995. Carbonate cement stratigraphy and timing of diagenesis in a miocene mixed carbonate-clastic sequence, offshore Sabah, Malaysia – constraints from cathodoluminescence, geochemistry, and isotope studies. Sed. Geol. 99, 191–214.

Ashirov, K.B., 1960. About Question of Time of Formation of Oil and Gas Fields in Middle Part of Volga River Region. Geologia nefti i gaza 6. (in Russian).

Bachtel, S.L., Dorobek, S.L., 1998. Mississippian carbonate ramp-to-basin transitions in south-central new Mexico: sequence stratigraphic response to progressively steepening outer-ramp profiles. J. Sed. Res. 68, 1189–1200.

Bodnar, R.J., Vityk, M.O., 1994. Interpretation of microthermometric data for H_2O-NaCl fluid inclusions. Fluid Incl. Min. Methods Appl. 117–130.

Bruckschen, P., Richter, D.K., 1994. Zementstratigraphische grundmuster in marinen

karbonatablagerungen des phanerozoikums – ein abbild der normalen Beckenentwicklung. Zentralbl. Geol. Paläontol. 1993, 959–972.
Bruckschen, P., Neuser, R.D., Richter, D.K., 1992. Cement stratigraphy in triassic and jurassic limestones of the weserbergland (northwestern Germany). Sed. Geol. 81, 195–214.
Buggisch, W., Wang, X., Alekseev, A.S., Joachimski, M.M., 2011. Carboniferous–permian carbon isotope stratigraphy of successions from China (Yangtze platform), USA (Kansas) and Russia (Moscow Basin and Urals). Palaeogeogr. Palaeoclim. Palaeoecol. 301, 18–38.
Burchette, T.P., Wright, V.P., 1992. Carbonate ramp depositional systems. Sed. Geol. 79, 3–57.
Burley, S.D., Mullis, J., Matter, A., 1989. Timing diagenesis in the tartan reservoir (UK North Sea): constraints from combined cathodoluminescence microscopy and fluid inclusions studies. Mar. Pet. Geol. 6, 98–120.
Burruss, R.C., Cercone, K.R., Harris, P.M., 1983. Fluid inclusion petrography and tectonic-burial history of the ali No. 2 well: evidence for timing of diagenesis and oil migration, northern Oman Foredeep. Geology 2, 567–570.
Byrnes, A.P., Bhattacharya, S., 2006. Influence of initial and residual oil saturation and relative permeability on recovery from transition zone reservoirs in shallow-shelf carbonates, SPE/DOE symposium on improved oil recovery. Soc. Pet. Eng. SPE 99736, http://dx.doi.org/10.2118/99736-MS.
Carnegie, A., 2006. Understanding the Pressure Gradients Improves Production from Oil/Water Transition Carbonate Zones, SPE 99240, Presented at the 2006 SPE, DOE. Symposium on Improved Oil Recovery, Tulsa, USA, pp. 22–26.
Carpentier, C., Brigaud, B., Blaise, T., Vincent, B., Durlet, C., Boulvais, P., Pagel, M., Hibsch, C., Yven, B., Lach, P., Cathelineau, M., Boiron, M., Landrein, P., Buschaertf, S., 2014. Impact of basin burial and exhumation on jurassic carbonates diagenesis on both sides of a thick clay barrier (Paris Basin, NE France). Mar. Pet. Geol. 53, 44–70.
Christ, N., Immenhauser, A., Amour, F., Mutti, M., Preston, R., Whitaker, F.F., Peterhänsel, A., Egenhoff, S.O., Dunn, P.A., Agar, S., 2012. Triassic latemar cycle tops - subaerial exposure of platform carbonates under tropical arid climate. Sed. Geol. 265–266, 1–29.
Christiansen, R., Heymans, M., Fanchi, J., 2000. Estimating oil reserves in oil-water transition zones, SPE Asia Pacific conference on integrated modelling for asset Management. Soc. Pet. Eng.
Cox, P.A., Wood, R.A., Dickson, J.A.D., Al Rougha, H.B., Shebl, H., Corbett, P.W.M., 2010. Dynamics of cementation in response to oil charge: evidence from a cretaceous carbonate field. U.A.E. Sed. Geol. 246–254.
Doveton, J.H., 1999. Basics of Oil & Gas Log Analysis, p. 34.
Ehrenberg, S.N., Pickard, N.A.H., Svånå, T.A., Oxtoby, N.H., 2002. Cement geochemistry of photozoan carbonate strata (upper carboniferous-lower permian), finmark carbonate platform, barents sea. J. Sed. Res. 72, 95–115.
Fanchi, J., Christiansen, R., Heymans, M., 2002. Estimating oil reserves of fields with oil/water transition zones. SPE Reserv. Eval. Eng. 5, 311–316. SPE 59352.
Galimov, E.M., Kamaleeva, A.I., 2015. Source of hydrocarbons in the supergiant romashkino oilfield (Tatarstan): recharge from the crystalline basement or source sediments? Eur. Spine J. 24, 95–112.
Goldstein, R.H., Reynolds, T.J., 1994. Systematics of Fluid Inclusions in Diagenetic Minerals: SEPM Short Course 31. Society for Sedimentary Geology, p. 199.
Gorbachev, Y.I., 1990. Geophysical Investigations of Wells. Nedra, p. 398 (in Russian).
Gordadze, G.N., Tikhomirov, V.I., 2005. Geochemical characteristics of oils and dispersed organic matter from the rocks of the central volga-ural basin: hydrocarbon biomarker data. Geochem. Int. 43 (11), 1108–1123.
Gorunova, L.F., 2009. Structure and Assessment of Prospects Oil and Gas Potential of Middle Devonian and Lower Carboniferous Oil Saturated Complexes Melekesskaya Depression. PhD dissertation. Kazan University, p. 150 (in Russian).
Granier, B., Staffelbach, C., 2009. Quick look cathodoluminescence analyses and their impact on the interpretation of carbonate reservoirs. Case study of mid-jurassic oolitic reservoirs in the Paris basin. Carn. Geol. Noteb. Geol. 6, 1–14.
Grossman, E.L., Bruckschen, P., Mii, H.S., Chuvashov, B.I., Yancey, T.E., Veizer, J., 2002. Carboniferous paleoclimate and global change: isotopic evidence from the Russian platform. carboniferous stratigraphy and paleogeography in Eurasia. Inst. Geol. Geochem. Russ. Acad. Sci. 61–71. Urals Branch, Ekaterinburg.
Hachatryan, R.O., 1979. Tectonic Development and Oil-and-gas Potential of the Volga-Kamsky Anticline. Science publications of the University of Kazan, p. 171 (in Russian).
Halymbadzha, V.G., 1962. Middle Carboniferous Rocks North, Central and West Districts Tatar Region. Kazan University press, p. 239 (in Russian).
Hao, F., Hao, F., Zhang, X.F., Wang, C.W., Li, P.P., Guo, T.L., Zou, H.Y., Zhu, Y.M., Liu, J.Z., Cai, Z.X., 2015. The fate of CO_2 derived from thermochemical sulfate reduction (TSR) and effect of TSR on carbonate porosity and permeability, sichuan basin, China. Earth Sci. Rev. 141, 154–177.
Heasley, E.C., Worden, R.H., Hendry, J.P., 2000. Cement distribution in a carbonate reservoir: recognition of a palaeo oil-water contact and its relationship to reservoir quality in the humbly grove field, onshore, UK. Mar. Pet. Geol. 17, 639–654.
Heckel, P.H., 1986. Sea-level curve for the pennsylvanian eustatic marine transgressive-regressive depositional cycles along midcontinent outcrop belt, north-America. Geology 14, 330–334.
Heggheim, T., Madland, M., Risnes, R., Austad, T., 2005. A chemical induced enhanced weakening of chalk by seawater. J. Pet. Sci. Eng. 46, 171–184.
Helgeson, H.C., Knox, A.M., Owens, C.E., Shock, E.L., 1993. Petroleum, oil field waters, and authigenic mineral assemblages: are they in metastable equilibrium in hydrocarbon reservoirs. Geochim. Cosmochim. Acta 57, 3295–3339.
Immenhauser, A., 2009. Estimating palaeo-water depth from the physical rock record. Earth Sci. Rev. 96, 107–139.
Immenhauser, A., Dublyansky, Y.V., Verwer, K., Fleitman, D., Pashenko, S.E., 2007. Textural, elemental and isotopic characteristics of pleistocene phreatic cave deposits (Jabal Madar, Oman). J. Sed. Res. 77, 68–88.
Ingalls, A.E., Aller, R.C., Lee, C., Wakeham, S.G., 2004. Organic matter diagenesis in shallow water carbonate sediments. Geochim. Cosmochim. Acta 68, 4363–4379.
Jesenius, J., Burruss, R.C., 1990. Hydrocarbon-water interactions during brine migration: evidence from hydrocarbon inclusions in calcite cements from danish North sea oil fields. Geochim. Cosmochim. Acta 54, 705–713.
Kaufman, J., Cander, H.S., Daniels, L.D., Meyers, W.J., 1988. Calcite cement stratigraphy and cementation history of the burlington-keokuk formations (mississippian) illinois and missouri. J. Sed. Pet. 58, 312–326.
Kaufmann, B., 1997. Diagenesis of middle devonian carbonate mounds of the mader basin (eastern anti-atlas, Morocco). J. Sed. Res. 67, 945–956.
Kerimov, V.Yu, Osipov, A.V., Lavrenova, E.A., 2014. The hydrocarbon potential of deep horizons in the south-eastern part of the volga-urals oil and gas province. Neft. khozyaystvo Oil Ind. 4, 33–35.
Khalil, M.I., Islam, F., Eunuse, A., 2015. Gamma and resistivity logs for characterization of gondwana coal seams at the northwestern part of Bangladesh. Arab. J. Geosci. 8, 6497–6506.
Kim, S.-T., O'Neil, J.R., 1997. Equilibrium and non-equilibrium oxygen isotope effects in synthetic carbonates. Geochim. Cosmochim. Acta 61, 3461–3475.
Kolchugin, A.N., Morozov, V.P., Korolev, E.A., Eskin, A.A., Gazeeva, F.M., 2013. Typical sections of bashkirian carbonate rocks and structure of oil deposits in southeast part of the Republic of Tatarstan. Neft. Khozyaistvo Oil Ind. 11, 84–86.
Mkrtchyan, O.M., 1980. Regularities of Structural Forms in the East of the Russian Plate. Science pub., p. 134 (in Russian).
Morrow, D.W., 1982. Diagenesis. Dolomite. Pt 2: dolomitization models and ancient dolostones. Geosci. Can. 9, 95–107.
Morrow, N.R., Mason, G., 2001. Recovery of oil by spontaneous imbibition. Curr. Opin. Coll. Interface Sci. 6, 321–337.
Neilson, J.E., Oxtoby, N.H., 2008. The relationship between petroleum, exotic cements and reservoir quality in carbonates – a review. Mar. Pet. Geol. 25, 778–790.
Neilson, J.E., Oxtoby, N.H., Simmons, M.D., Simpson, I.R., Fortunatova, N.K., 1998. The relationships between petroleum emplacement and carbonate reservoir quality: examples from abu dhabi and the amu darya Basin. Mar. Pet. Geol. 15, 57–72.
Proust, J.N., Chuvashov, B.I., Vennin, E., Boisseau, T., 1998. Carbonate platform drowning in a foreland setting: the mid-carboniferous platform in western urals (Russia). J. Sed. Res. 68, 1175–1188.
Richter, D.K., Götte, T., Götze, J., Neuser, R.D., 2003. Progress in application of cathodoluminescence (CL) in sedimentary petrology. Mineral. Pet. 79, 127–166.
Risnes, R., Haghighi, H., Korsnes, R., Natvik, O., 2003. Chalk–fluid interactions with glycol and brines. Tectonophysics 370, 213–226.
Risnes, R., Madland, M., Hole, M., Kwabiah, N., 2005. Water weakening of chalk—mechanical effects of water–glycol mixtures. J. Pet.. Sci. Eng. 48, 21–36.
Sathar, S., Worden, R.H., Faulkner, D.R., Smalley, P.C., 2012. The effect of oil saturation on the mechanism of compaction in granular materials: higher oil saturations lead to more grain fracturing and less pressure solution. J. Sed. Res. 82, 571–584.
Sellwood, B.W., Wilkes, M., James, B., 1993. Hydrocarbon inclusions in late calcite cements: migration indicators in the great oolite group, weald basin, southern England. Sed. Geol. 84, 51–55.
Sharkov, E., Lebedev, V., Chugaev, A., Zabarinskaya, L., Rodnikov, A., Sergeeva, N., Safonova, I., 2015. The caucasian-arabian segment of the alpine-himalayan collisional belt: geology, volcanism and neotectonics. Geosci. Front. 6, 513–522.
Shepherd, T.J., Rankin, A.H., Alderton, D.H.M., 1985. A Practical Guide to Fluid Inclusion Studies. Blackie & Son, Glasgo, p. 239.
Simo, J.A., Lehmann, P.J., 2000. Diagenetic history of pipe creek JR reef, silurian, north-central indiana, U.S.A. J. Sed. Res. 70, 937–951.
Soreghan, G.S., Giles, K.A., 1999. Amplitudes of late pennsylvanian glacioeustasy. Geology 27, 255–258.
Steele-MacInnes, M., Bodnar, R.J., Naden, J., 2011. Numerical model to determine the composition of H_2O-NaCl-$CaCl_2$ fluid inclusions based on microthermometric and microanalytical data. Geochim. Cosmochim. Acta 75, 21–40.
Steinhauff, D.M., Kenneth, R.W., Goldberg, S.A., 1999. Diagenesis by burial fluids, middle Ordovician platform-margin limestones, East Tennessee: relationships to Mississippi valley-type deposits. J. Sed. Res. 69, 1107–1122.
Swart, P.K., 2015. The geochemistry of carbonate diagenesis: the past, present and future. Sedimentology 62, 1233–1304.
Ten Have, T., Heijnen, W., 1985. Cathodoluminescence activation and zonation in carbonate rocks – an experimental approach. Geol. Mijnb. 64, 297–310.
Voytovich, E.D., Gatiyatullin, N.S., 2003. Tectonics of Tatarstan. Kazan University press, p. 132 (in Russian).
Walkden, G.M., Williams, D.O., 1991. The diagenesis of the late dinantian derbyshire-East midland carbonate shelf, central England. Sedimentology 38, 643–670.
Walter, B.F., Immenhauser, A., Geske, A., Markl, G., 2015. Exploration of hydrothermal carbonate magnesium isotope signatures as tracers for continental fluid aquifers, schwarzwald mining district, SW Germany. Chem. Geol. 400, 87–105.
Worden, R.H., Heasley, E.C., 2000. Effects of petroleum emplacement on

cementation in carbonate reservoirs. Bull. Soc. Geol. Fr. 171, 607–620.
Worden, R.H., Oxtoby, N.H., Smalley, P.C., 1998. Can oil emplacement prevent quartz cementation in sandstones? Pet. Geosci. 4, 129–137.
Worden, R.H., Heasley, E.C., Barclay, S.A., 1999. The effects of petroleum emplacement on diagenesis: a comparison between sandstone and carbonate reservoirs. In: Sciences Geologiques, 100. Mem, Strasbourg.
Yudina, A.B., Racki, G., Savage, N.M., Racka, M., Małkowski, K., 2002. The frasnian-famennian events in a deep-shelf succession, subpolar urals: biotic, depositional, and geochemical records. A. Palaeont. Pol. 47, 355–372.
Zeeh, S., Bechstädt, T., McKenzie, J., Richter, D.K., 1995. Diagenesis evolution of the carnian wetterstein platforms of the eastern alps. Sedimentology 42, 199–222.
Zhang, P.M., Tweheyo, M.T., Austad, T., 2007. Wettability alteration and improved oil recovery by spontaneous imbibition of seawater into chalk: impact of the potential determining ions Ca^{2+}, mg (2+), and SO^4_2. Coll. Surf. A Physicochem. Eng. Asp. 301, 199–208.